

# Spin valve sensors for ultrasensitive detection of superparamagnetic nanoparticles for biological applications

Guanxiong Li<sup>a</sup>, Shouheng Sun<sup>b</sup>, Robert J. Wilson<sup>a</sup>, Robert L. White<sup>a</sup>,  
Nader Pourmand<sup>c</sup>, Shan X. Wang<sup>a,\*</sup>

<sup>a</sup> Department of Materials and Engineering, Stanford University, Stanford, CA 94305-4045, USA

<sup>b</sup> Department of Chemistry, Brown University, Providence, RI 02912, USA

<sup>c</sup> Stanford Genome Technology Center, Stanford University, 855 California Avenue, Palo Alto, CA 94304, USA

Received 2 June 2005; received in revised form 7 September 2005; accepted 2 October 2005

Available online 2 November 2005

## Abstract

We present giant magnetoresistance (GMR) spin valve sensors designed for detection of superparamagnetic nanoparticles as potential biomolecular labels in magnetic biodetection technology. We discuss the sensor design and experimentally demonstrate that as few as ~23 monodisperse 16-nm superparamagnetic Fe<sub>3</sub>O<sub>4</sub> nanoparticles can be detected by submicron spin valve sensors at room temperature without resorting to lock-in detection. A patterned self-assembly method of nanoparticles, based on a polymer-mediated process and fine lithography, is developed for the detection. It is found that sensor signal increases linearly with the number of nanoparticles.

© 2005 Elsevier B.V. All rights reserved.

**Keywords:** Spin valve sensor; GMR; Magnetic nanoparticle; Biodetection; Biosensor

## 1. Introduction

For the past several years, giant magnetoresistance (GMR)-based magnetic biodetection technology, which involves labeling biomolecules with magnetic micro- or nanometer-sized particles and detecting the magnetic fringing fields of the particle labels by GMR sensors after capture by target-probe biomolecular recognition, has received increasing research and development efforts [1–14]. This is because the GMR biosensors are promising for sensitive, large-scale, inexpensive, and portable biomolecular identification. They are also compatible with standard silicon IC technology, and suitable for integration into a lab-on-chip system. Compared to the superconducting quantum interference device (SQUID)-based ultrasensitive magnetic biodetection [15,16], the GMR technology has advantages of room-temperature operation, less complex instruments, and hence more portable and flexible implementation. Moreover, given the nature of the solid-state thin film sensors and the IC compatible fabrication, the GMR biosensors can be integrated

into a very high density, individually addressable array similar to the magnetic random access memory (MRAM), and hence such a GMR sensor array will be well suited for multi-analyte biodetection [2,3].

Up to date, most magnetic particle labels in the literature are micron or submicron sized, usually composed of a polymer matrix with imbedded magnetic nanoparticles or a polymer core coated with magnetic nanoparticles [1–10]. However, in order to achieve ultrahigh biodetection sensitivity, e.g., single molecule detection, the dimension of magnetic particle labels should be comparable to that of biomolecules. In the case of detecting DNA fragments, it is ideal to have the particle labels at 20 nm or smaller in diameter [17]. Such small nanoparticles would not block bimolecular interactions, such as hybridization between complementary gene fragments. Moreover, one nanoparticle label may be conjugated with one or at most a few DNA fragments, which will help establish a quantitative relationship with a sufficient accuracy between the number of captured particle labels and the actual biorecognition events. In contrast, it is quite difficult to do so with microbeads because of their large size mismatch with biomolecules. The monodispersity of crystalline magnetic nanoparticles in both size and magnetic moment [18,19] also benefits the signal quantification,

\* Corresponding author. Tel.: +1 650 723 8671; fax: +1 650 215 9918.  
E-mail address: [sxwang@stanford.edu](mailto:sxwang@stanford.edu) (S.X. Wang).

in contrast to the large variations of the microbeads in magnetic moment [1,10].

Given all these desirable properties, magnetic nanoparticles with a diameter of 20 nm or smaller become desirable biomolecular labels for ultrasensitive, highly quantitative magnetic biodetection technology. On the other hand, such tiny magnetic nanoparticles are a great challenge to the detectors, because their magnetic moments are very low due to their limited physical volume, relatively large surface area, and significant thermal disturbance to magnetic moments, i.e., superparamagnetism. In this paper, we present a GMR spin valve sensor designed and fabricated for detecting monodisperse superparamagnetic nanoparticles as potential biomolecular labels. The sensor design will be discussed first, and then we will present experimental results demonstrating the quantitative detection of a few tens to hundreds of magnetic nanoparticles (16-nm  $\text{Fe}_3\text{O}_4$ ) by spin valve sensors at room temperature.

## 2. Sensor design

### 2.1. Spin valve sensor

The physical volume of magnetic nanoparticles limits their magnetic moments and hence their magnetic fringing fields. Therefore, the nanoparticle sensor is required to possess high field sensitivity. For that reason, a GMR spin valve has been chosen as the sense element for magnetic nanoparticle detection because of its high sensitivity to low magnetic fields [20]. The spin valve with a synthetic antiferromagnet pinned layer is the preferred structure for its large dynamic range of field, good thermal stability, and design flexibility [21], and is actually used to fabricate the spin valve sensors presented in this paper.

Fig. 1 shows schematic drawings of a spin valve sensor designed for detecting magnetic nanoparticles that are conceptually immobilized onto the sensor surface via DNA hybridization. Unlike the binary digital output of a spin valve cell in nonvolatile memory applications [22], a linear analog signal is desired from the spin valve sensors for quantitative biodetection. For this purpose, the spin valve sensor is best configured in an orthogonal magnetization state [23]. Fig. 1(a) shows a patterned rectangular spin valve sensor with its pinned magnetization  $M_p$  fixed in the transverse or  $y$  direction and the free magnetization  $M_f$  rotating freely in the sensor plane. In this configuration, the sensor resistance can be expressed as  $R = R_0 + (1/2)\Delta R_{\max} \sin \theta_f$ , where  $\Delta R_{\max} = R_{\text{AP}} - R_p$  is the sensor resistance change between the antiparallel ( $R_{\text{AP}}$ ) and parallel ( $R_p$ ) magnetization configurations,  $R_0 = R_p + \Delta R_{\max}/2$  is the sensor resistance at the orthogonal configuration, and  $\theta_f$  is the orientation angle of free layer magnetization with respect to the longitudinal or  $x$  direction. For an external field applied in the transverse direction within a certain range,  $\sin \theta_f$  is linear or approximately linear with the field, leading to a linear dependence of sensor resistance on the field too.

For our spin valve sensors, a couple of methods have been used to establish such an orthogonal magnetization configuration. We deposited the free and pinned layers in different magnetic fields that were orthogonal to each other. Moreover,

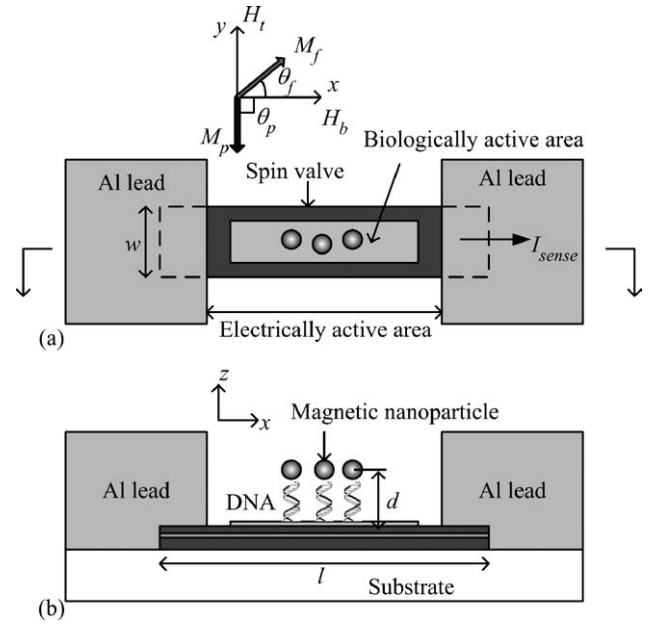


Fig. 1. Schematic illustrations of (a) the top view of a spin valve sensor and (b) its cross-section. A few magnetic nanoparticle labels are conceptually shown bound to the sensor through hybridized probe and target DNAs in the biologically active area.  $M_f$  and  $M_p$  are the free and pinned magnetization of the spin valve sensor, respectively.  $H_t$  and  $H_b$  are the applied magnetic excitation and bias fields, respectively.

as shown in Fig. 1(a), the sensors were patterned in such a rectangular shape that the pinned magnetization is aligned in the transverse direction and the shape anisotropy will then align the free layer magnetization in the longitudinal direction. In this magnetic configuration, the transverse direction is the field-sensitive direction of the spin valve sensors.

To avoid unwanted Barkhausen noise in the signal output of a spin valve sensor, we need to magnetically stabilize the sensing free layer. As used in magnetic recording heads, a permanent magnet bias would be effective for free layer stabilization for the spin valve biosensor, but with a modest increase in fabrication complexity. For our prototype spin valve sensors, especially those with a submicron-scale width ( $w$ ), we utilize shape anisotropy to stabilize the free layer. In addition, an external bias field  $H_b$ , as shown in Fig. 1(a), can also be applied to enhance the free layer stabilization. Moreover, we overlay thick aluminum leads on the end segments of the spin valve stripe where complex domain structure is most likely to form, as shown in Fig. 1. This lead configuration will shunt the electrical sense current ( $I_{\text{sense}}$ ) away from those regions and hence reduce possible Barkhausen noise.

Defined by the aluminum leads, the central segment of a spin valve sensor generates the electrical signal when a sense current passes through it, and therefore is called the “electrically active area”. When designing the electrically active area, we should consider the sensor surface area available for biochemical reactions, which is called the “biologically active area”, the sensor signal strength, and noise. As illustrated in Fig. 1, the biologically active area is an area of the surface located inside the electrically active area and where biorecognition, such as DNA

hybridization, and nanoparticle immobilization occurs. The biologically active area can be a physically separate layer, such as gold, deposited on the sensor to suit the surface chemistry requirements for biochemical reactions. In principle, the biologically active area can be as large as the whole electrically active area to maximize the available biochemical reaction sites. However, for good signal quantification, the biologically active area should rather be confined to the central portion of the electrically active area and have a high aspect ratio, because the spatial uniformity of the sensor signal degrades significantly when magnetic nanoparticles are located close to the sensor edges [12]. Nonetheless, given a sensor width, the longer the electrically active length is, the larger the biologically active area can be.

A long electrically active length is also beneficial to the sensor signal, because the longer the electrically active length is, the more magnetic flux from magnetic nanoparticles the electrically active area collects, and therefore the larger the sensor signal is due to the nanoparticles. On the other hand, the sensor noise increases with the electrically active length, because electrical noises, such as  $1/f$  noise and Johnson noise increase with the sensor resistance which is proportional to the electrically active length. Therefore, the electrically active length should be a result of balancing all these factors. Similar trade-off exists to the sensor width. It is straightforward to see that the narrower the sensor width is, the more sensitive the sensor is to the magnetic fields of the nanoparticles. However, narrowing sensor width will increase sensor resistance and hence noise, and also decrease the biologically active area.

## 2.2. Detection methods

The basic idea of detecting magnetic nanoparticle labels is to excite the superparamagnetic nanoparticles with a magnetic field and then to detect their magnetic responses (moments or fields) by the GMR sensors [1–13]. The magnetic excitation field, however, can be applied in different forms and directions. For example, a DC or AC magnetic excitation field can be applied, and this excitation field can be either in the sensor plane or perpendicular to the sensor plane, leading to four detection modes: in-plane DC [4,6,8,13], in-plane AC [7], vertical DC [5,10], and vertical AC modes [1–3,12], as illustrated in Fig. 2 where the excitation field is denoted as  $H_t$ . In addition to the excitation field, a constant DC bias field  $H_b$  may also be applied in the sensor plane for different purposes in different detection modes. In this paper, we define the sensor's response to the excitation field  $H_t$  as the sensor signal. The static DC bias field  $H_b$  only affects the base state of the spin valve sensor.

As shown in Fig. 2(a and c), in the in-plane detection modes, the magnetic excitation field  $H_t$  is applied in the transverse direction, which is the field-sensitive direction of the spin valve sensor, and the DC magnetic bias field  $H_b$ , if applied, is in the longitudinal direction. The DC bias field  $H_b$  has three roles in the in-plane modes: (1) stabilizing the free layer in the spin valve sensor, (2) defining a proper working point for the sensor, and (3) providing an initial polarization or magnetization for nanoparticles. However, for the in-plane detection modes, the bias field is not really necessary if other free layer stabilization methods,

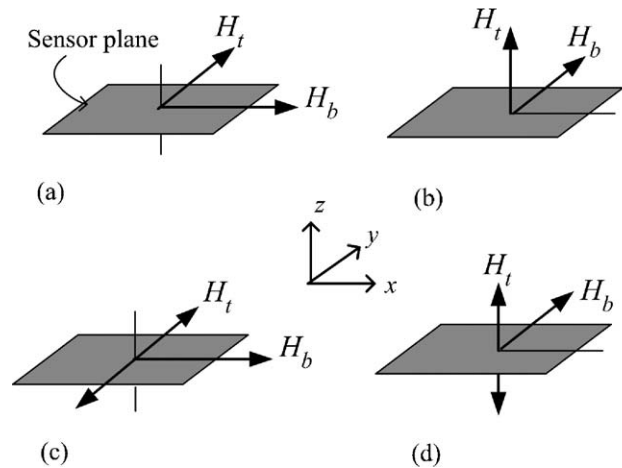


Fig. 2. Schematic illustrations of four nanoparticle detection modes: (a) in-plane DC mode, (b) vertical DC mode, (c) in-plane AC mode, and (d) vertical AC mode, corresponding to the four combinations of the direction and form of the magnetic excitation field  $H_t$ .  $H_b$  is a constant DC bias field applied in the sensor plane. A double-head arrow indicates an AC field, while a single-head arrow indicates a DC field.

such as permanent magnet bias or a large shape anisotropy, are available. In fact, the application of  $H_b$  in the longitudinal direction will decrease the field sensitivity of the spin valve sensor in the transverse direction, because  $H_b$  will increase the magnetic stiffness of the free layer magnetization. Moreover, the magnetic nanoparticles do not need an initial polarization in the in-plane modes, because the excitation field  $H_t$  is already in the transverse direction and the induced effective magnetic fields from the nanoparticles will also be exerted in the same direction on the sensor. Based on the above reasons, the DC bias field may be needed only for a micron-wide spin valve sensor, mainly to stabilize its free layer, whereas for a submicron-wide sensor it may not be needed if the free layer is already in a single domain state.

For the vertical modes, the excitation field  $H_t$  is applied in the vertical direction. The DC bias field, however, needs to be applied in the transverse direction for a spin valve sensor [12], as shown in Fig. 2(b and d). In contrast to GMR multilayer sensors whose resistance is affected only by the field magnitude [1–3,5,10], a spin valve sensor is sensitive to the field direction as well. If no DC bias field is applied, the magnetic fringing field of a vertically magnetized nanoparticle will be radially symmetrical in the sensor plane [24], leading to a zero net field. This is not a problem for a GMR multilayer sensor, but it is an important issue for a spin valve sensor because the resistance of a spin valve sensor under such a radially symmetrical field will not change. However, we know that the magnetic susceptibility ( $\chi$ ) of superparamagnetic nanoparticles is not constant but a function of applied field  $H$ , i.e.,  $\chi(H) = M/H = m_s L(\alpha) / HV_p$ , where the Langevin function  $L(\alpha) = \coth \alpha - 1/\alpha$ ,  $\alpha = m_s H / kT$ ,  $m_s$  is the saturation moment of a nanoparticle,  $V_p$  the nanoparticle's volume,  $k$  the Boltzmann's constant, and  $T$  is the temperature. Therefore, by applying a transverse bias field  $H_b$  in the vertical detection modes, we can not only gain a nonzero transverse magnetic moment  $m_y = \chi(H = \sqrt{H_b^2 + H_t^2}) H_b V_p$  for the nanoparticle,

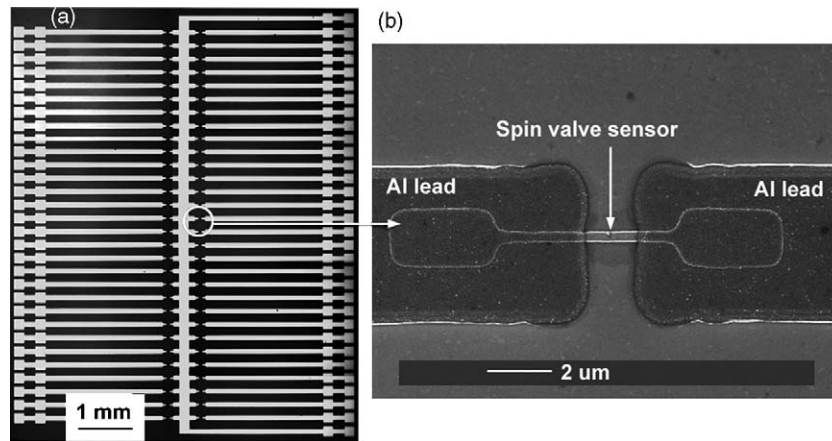


Fig. 3. (a) An optical micrograph of a fabricated spin valve sensor array of 60 sensors on a  $\sim 7$  mm  $\times$  8 mm chip and (b) the scanning electron microscope (SEM) image of one submicron sensor in the array.

but also make this transverse moment vary with the vertical excitation field  $H_t$  via the field-dependent magnetic susceptibility  $\chi$ . Hence, due to this transverse moment, the average in-plane field from the nanoparticle will also vary with  $H_t$ . As a result, the resistance of the spin valve sensor with captured nanoparticles will change in response to the vertical excitation field. For the above reasons, a transverse DC bias field is indispensable in the vertical detection modes for a spin valve sensor.

One advantage of the vertical modes over the in-plane modes is that there is no net signal output when no magnetic nanoparticles are present, because a spin valve sensor is insensitive to a vertical excitation field. On the other hand, the in-plane modes have a higher tolerance to the possible misorientation of the excitation field  $H_t$  than the vertical modes due to the same reason. A slight tilting out of the sensor plane of  $H_t$  would not affect the sensor signal much because of the insensitivity of the spin valve to the vertical field. In the vertical modes, however, a slight tilting of  $H_t$  away from the normal direction will introduce an in-plane component of  $H_t$ , which would, in turn, change the zero-particle signal from null to a finite value that might be comparable to the true signal from the nanoparticles.

As mentioned before, the magnetic excitation field  $H_t$  can be DC or AC. Compared to a DC excitation, an AC excitation will generate an AC MR signal from a spin valve sensor, which therefore can be measured with a lock-in amplifier to achieve a high signal-to-noise ratio (SNR) [1–3,7,9,12]. The in-plane AC mode signal has the same frequency ( $1f$ ) as the AC excitation field  $H_t$  [7], whereas the vertical AC mode signal is at twice the frequency ( $2f$ ), because the upward and downward half periods of  $H_t$  have the same effect on changing the transverse magnetic field of the nanoparticles in a spin valve sensor with a DC transverse bias field  $H_b$  [12]. In contrast to a DC magnetic excitation, an AC magnetic excitation will introduce electromagnetic interference (EMI) to the sensor signal, because the AC field will cause a time-varying magnetic flux in the measurement circuit which, in turn, generates an AC voltage as governed by the Faraday's law. This EMI can easily surpass the true signal from the nanoparticles and therefore extra care is needed in the AC mode detection.

For the nanoparticle detection demonstrated in this paper, we have chosen the in-plane DC mode for its EMI-free signal, the easiness of magnetic field alignment, and the simple measurement setup, for which only the transverse excitation field  $H_t$  is needed.

### 3. Magnetic nanoparticle detection

#### 3.1. Sensor fabrication

The spin valve sensors with synthetic pinned layers and a magnetoresistance (MR) ratio of 11.3% were fabricated at submicron scale by e-beam lithography with a width of about  $0.2 \mu\text{m}$ . Reducing sensor width from micron to submicron size will increase the effective field of the magnetic nanoparticles in the sensor and therefore enhance the sensor's detection sensitivity [7,11–13]. The sensor fabrication started with the spin valve thin film deposition on a 4-in. silicon wafer with the pinned magnetization ( $M_p$ ) set in a selected direction. This selected direction will make  $M_p$  aligned in the width or transverse ( $y$ ) direction of the patterned spin valve sensors, as illustrated in Fig. 1(a). e-Beam lithography (Hitachi HL-700F) was used to pattern sensor stripes on a submicron scale. The patterns were thereafter transferred into the spin valve thin film by timed ion milling. After stripping off the e-beam resist, optical lithography (Electronic Visions 620 Aligner) was used to overlay leads pattern on the spin valve sensor stripes. Thick (300 nm) aluminum layer was then deposited on the wafer by ion beam deposition. Electrical leads and pads to the spin valve sensors were formed after lift-off. Fig. 3 shows (a) the optical micrograph of a fabricated spin valve sensor array of 60 sensors on a  $\sim 7$  mm  $\times$  8 mm chip and (b) the scanning electron microscope (SEM) image of one submicron sensor in the array.

#### 3.2. Magnetic nanoparticles

Monodisperse 16-nm  $\text{Fe}_3\text{O}_4$  nanoparticles are used in the magnetic nanoparticle detection experiments [19]. The left inset in Fig. 4 shows a SEM image of the nanoparticles. At room tem-

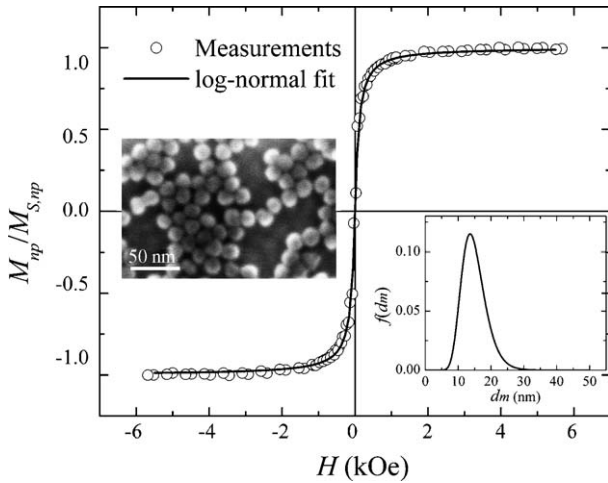


Fig. 4. Normalized magnetization curves of 16-nm  $\text{Fe}_3\text{O}_4$  nanoparticles measured by VSM at room temperature. The left inset shows the SEM image of the nanoparticles. The right inset is the distribution of particle magnetic diameter obtained from the log-normal fitting to the magnetization curve.

perature, the 16-nm  $\text{Fe}_3\text{O}_4$  nanoparticles are superparamagnetic, as indicated by the magnetization curve shown in Fig. 4, which is measured with a vibrating sample magnetometer (VSM). Also shown in Fig. 4 is the fitting of the magnetization curve with the Langevin function weighted by a log-normal distribution of nanoparticle diameter [25,26]:

$$\frac{M_{np}}{M_{S,np}} = \frac{\int_0^\infty L(\alpha) f(d_m) dd_m}{\int_0^\infty f(d_m) dd_m}, \quad (1)$$

where  $L(\alpha)$  is the Langevin function with  $\alpha = m_s H/kT$ ,  $d_m$  the effective magnetic diameter of nanoparticle, and  $f(d_m)$  is the log-normal distribution of the magnetic diameter:

$$f(d_m) = \frac{1}{\sqrt{2\pi} d_m \sigma_d} \exp\left(-\frac{\ln^2(d_m/d_{m0})}{2\sigma_d^2}\right), \quad (2)$$

where  $d_{m0}$  is the median diameter and  $\sigma_d$  is the distribution width. The particle moment  $m_s$  is related to the magnetic diameter as  $m_s = \pi d_m^3 M_S/6$ , where  $M_S = 480 \text{ emu/cm}^3$  is the saturation magnetization of  $\text{Fe}_3\text{O}_4$ , and the imperfection of a nanoparticle is represented by its reduced magnetic diameter with respect to its physical diameter. As we can see, the magnetization curve is well fitted by the weighted Langevin function, indicating the superparamagnetism of the nanoparticles. The particle diameter distribution is also plotted in the right inset of Fig. 4, for which  $d_{m0} = 14.5 \text{ nm}$  and  $\sigma_d = 0.25$ . The mean diameter of the  $\text{Fe}_3\text{O}_4$  nanoparticles is  $\bar{d}_m = d_{m0} e^{\sigma_d^2/2} = 14.9 \text{ nm}$ , close to the physical diameter of 16 nm as measured by transmission electron microscope (TEM) [19].

### 3.3. Experimental methods

In order to place magnetic nanoparticles on spin valve sensors, we developed a “bilayer lift-off” process to deposit the nanoparticles site-specifically. As schematically shown in Fig. 5(a), the bilayer lift-off process involves four steps: a bilayer of poly(ethylenimine) (PEI)/poly(methyl methacrylate) (PMMA) is sequentially coated onto the sensor surface (step 1). PEI is a functional polymer on which magnetic nanoparticles can self-assemble into a monolayer via ligand exchange between PEI

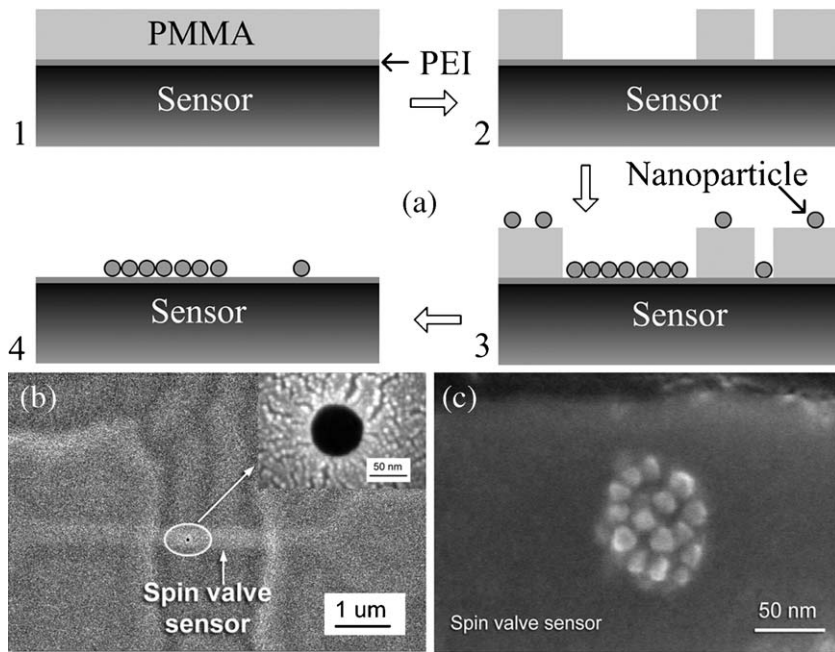


Fig. 5. (a) Schematic bilayer lift-off process: (1) a PEI/PMMA bilayer is sequentially coated on a sensor surface, (2) deposition areas are created in the PMMA layer by e-beam lithography, (3) magnetic nanoparticles self-assemble on exposed PEI layer in the deposition areas, and (4) the resist layer and unwanted nanoparticles are lifted off by solvent. (b) SEM image of a nanometer-scale dot patterned in the PMMA bilayer on a spin valve sensor. Inset shows the close-up of the dot. (c) Sixteen-nanometer  $\text{Fe}_3\text{O}_4$  nanoparticles deposited in such a dot pattern as shown in (b) after lift-off of the PMMA layer.

and the surface surfactant (oleic acid) of the nanoparticles [27]. The PEI layer of  $\sim 2$  nm thickness is dip-coated in chloroform solution. The e-beam resist layer PMMA is spin-coated on top of the PEI, and then the deposition areas are cleared by e-beam lithography (Raith 150) (step 2). After that, magnetic nanoparticles are applied in hexane solution onto the sensor surface. Some particles self-assemble on the exposed PEI layer in the deposition areas (step 3). Finally, the PMMA layer is stripped off with acetone and any nanoparticles on the PMMA layer are lifted off, leaving behind the self-assembled magnetic nanoparticles bound onto the PEI layer in the deposition area (step 4). For example, Fig. 5(b) shows a nanometer-scale dot pattern in the PMMA layer on a spin valve sensor and Fig. 5(c) shows 16-nm  $\text{Fe}_3\text{O}_4$  nanoparticles deposited in such a dot area after lift-off of the PMMA layer. By varying the size, location of deposition area and the concentration of nanoparticles in solution, we gain control of the number and position of deposited nanoparticles, which enables us to perform quantitative detection of magnetic nanoparticles on spin valve sensors.

The magnetic nanoparticle detection is performed in the in-plane DC mode with the magnetic excitation field  $H_t$  applied in the transverse direction (see Fig. 2(a)). In this work, no bias field  $H_b$  was applied for the submicron spin valve sensors due to their large shape anisotropy. The MR transfer curves, i.e., the sensor resistance versus the applied field  $H_t$ , are measured for the sensor with and without magnetic nanoparticles. The difference of the MR transfer curves indicates the presence and, further, the quantity of the captured nanoparticles.

We first patterned the nanoparticle deposition areas with varying sizes on a series of spin valve sensors on a chip like the one shown in Fig. 3(a). Then the sensor chip was brought to a probe station equipped with a homemade electromagnet and four tungsten probes. Driven by a DC power supply, the electromagnet supplied the magnetic excitation field  $H_t$  in the transverse direction of the spin valve sensors. The four tungsten probes were put in contact with the aluminum pads (see Fig. 3) to implement the four-probe measurement of the sensor resistance. A sense current of  $I_{\text{sense}} = -0.1$  mA was sourced to a spin valve sensor by a Keithley 236 Source-Measure Unit where the negative current runs in the  $-x$  direction (see Fig. 1(a)), while the voltage across the sensor was measured by a HP 3685 Multimeter. Both the magnetic field application and the sensor resistance measurement were controlled by a computer.

The 16-nm  $\text{Fe}_3\text{O}_4$  nanoparticles, in hexane dispersion, were then applied onto the sensor surface. After drying, the PMMA layer was lifted off with acetone. As a result of the varying size of the nanoparticle deposition areas, the  $\text{Fe}_3\text{O}_4$  nanoparticles were deposited in different quantities on different sensors. However, some sensors on the chip were intentionally skipped during the e-beam lithography so that they have no deposition area and hence no nanoparticles on surface. The sensors with deposited nanoparticles are called “detection sensors” and the ones without nanoparticles “reference sensors”. During the nanoparticle deposition, the sensor chip remained immobile at the probe station. The MR transfer curves were measured again after applying the nanoparticles. Comparing these two transfer curves gives the resistance differences caused by the deposited nanoparticles

$\Delta R = R_{\text{with}} - R_{\text{without}}$ , where  $R_{\text{with}}$  and  $R_{\text{without}}$  are the sensor resistances with and without nanoparticles, respectively.

### 3.4. Detection results and discussions

Fig. 6(a) shows the resistance differences of three detection sensors (filled symbols) and two reference sensors (open symbols) as examples of the series of measurements. There are increasing numbers of  $\text{Fe}_3\text{O}_4$  nanoparticles on detection sensors 1–3. Fig. 6(b and c) shows the SEM images of the detection sensors 1 and 2 with the deposited nanoparticles, respectively. The MR transfer curves before and after depositing the  $\text{Fe}_3\text{O}_4$  nanoparticles of the detection sensor 3 are also shown in the inset of Fig. 6(a). Due to the small effect of the nanoparticles, the resistance differences do not look as apparent on the MR transfer curves as on the  $\Delta R$  curves. The difference between the detection sensors and the reference sensors is readily noted in Fig. 6(a). Whereas the resistance differences of the reference sensors are almost flat around zero, the  $\Delta R$  curves of the detection sensors show two peaks, one negative for positive  $H_t$  and the

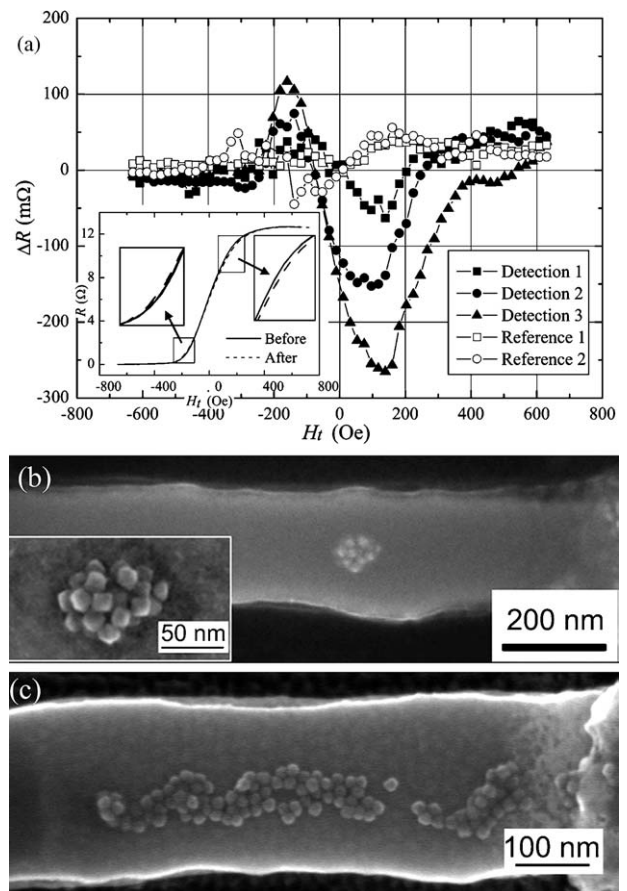


Fig. 6. (a) Resistance differences before and after depositing 16-nm  $\text{Fe}_3\text{O}_4$  nanoparticles for three detection sensors (filled symbols) and two reference sensors (open symbols). The inset shows the MR transfer curves measured before (solid line) and after (dashed line) the nanoparticle deposition for the detection sensor 3. The three detection sensors have different numbers of the  $\text{Fe}_3\text{O}_4$  nanoparticles. SEM images of (b) the detection sensor 1 with  $\sim 23$  deposited  $\text{Fe}_3\text{O}_4$  nanoparticles that are also shown in the inset at a higher magnification and (c) the detection sensor 2 with  $\sim 108$  nanoparticles.

other positive for negative  $H_t$ . The appearance of the peaks is the result of two competing factors: the sensor sensitivity and the nanoparticle fields. When the applied field  $H_t$  decreases from saturating values, the field sensitivity of the sensor increases until it reaches the maximum at low field, as seen in the MR transfer curves. On the other hand, the polarization and therefore the field of the nanoparticles decreases with the decreasing  $H_t$ . Hence, the MR effect of the nanoparticles peaks at some field in between the saturation and zero. The opposite polarity of the peaks is due to the fact that the field from the nanoparticles is opposite to the applied field on the sensors.

Spaced by  $\sim 2$ -nm thick PEI layer and  $\sim 5$ -nm spin valve capping layer, the 16-nm  $\text{Fe}_3\text{O}_4$  nanoparticles are about 7 nm above the free layer. At such a close distance, the magnetic stray field from the sensors will affect the polarization of the nanoparticles. The stray field comes from the ferromagnetic layers in the spin valve and from the sense current. The free layer stray field further interacts with the particle field during the detection. As a result of the influence of the sensor stray field, the positive and negative peaks in the  $\Delta R$  curves need not be symmetric about zero applied field. Indeed, some shifts of the zero-crossing point are observed on the  $\Delta R$  curves. The shifts are towards negative  $H_t$  in the  $-y$  direction, indicating that the stray field from the spin valve sensors at zero applied field is positive, in the  $+y$  direction. This positive sensor stray field may come from the negatively pinned moments, the free layer moment tilted negatively due to the interlayer coupling, and the sense current running in the  $-x$  direction. In another set of detection experiments, we intentionally moved the nanoparticles away from the sensor top to the sensor side at a large distance (a few hundred nanometers). A much smaller shifting was then observed because of the reduced sensor stray field at the greater distance.

Fig. 7 shows the peak-to-peak resistance difference  $\Delta R_{p-p}$  versus the number of deposited  $\text{Fe}_3\text{O}_4$  nanoparticles. The particles are counted on the SEM images. The solid line is a linear fit to the data. The horizontal dashed line indicates the fluctuation range of reference sensor signals, and may be considered the noise level of this detection method. Each data point corre-

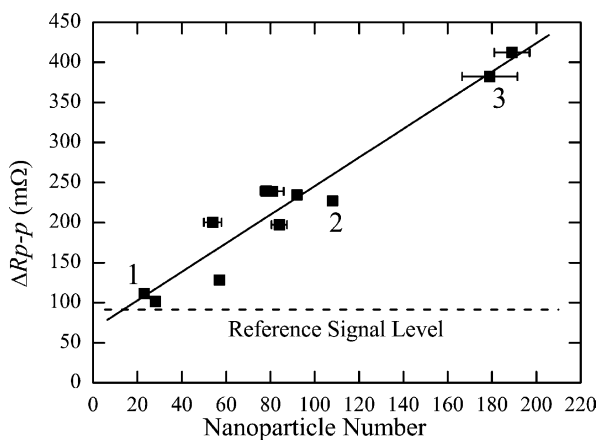


Fig. 7. The peak-to-peak resistance difference vs. the number of the deposited  $\text{Fe}_3\text{O}_4$  nanoparticles. The three detection sensors in Fig. 6(a) are explicitly labeled. The solid line is a linear fit and the dashed horizontal line designates the average signal fluctuation range of the reference sensors.

sponds to one detection sensor on the chip. The three detection sensors (1–3 in Fig. 6(a)) are explicitly labeled. In Fig. 7 we notice that the sensor signal  $\Delta R_{p-p}$  increases with the number of nanoparticles in a reasonably linear manner. The data scatter seen in Fig. 7 may be caused by the factors, such as the varying locations and distributions of nanoparticles on the sensors. Although the  $\text{Fe}_3\text{O}_4$  nanoparticles have a narrow size distribution [19], they are not identical, as seen in Fig. 4. This small distribution would also have an adverse impact on the sensor signal quantification, especially when the nanoparticle number is small as in this case. The sensor-to-sensor variation, such as physical dimension and field sensitivity, may contribute to the data scatter as well. Hence, it is foreseeable that the data scatter can be reduced by varying and counting nanoparticles on the same sensor for more realistic biodetection. In the current experiments, however, the deposited nanoparticles are strongly bound to the PEI layer so that the detection can only be performed once per sensor. Nonetheless, since these sensors are fabricated on the same chip and have closely similar properties, Fig. 7 represents to a large extent the sensor signal dependence on the nanoparticle quantity.

The fitting line in Fig. 7 intersects the reference signal level at 14 nanoparticles, which may be the minimum detectable number of nanoparticles in this detection scheme with a signal-to-noise ratio of  $\sim 1$ . The inferred 14 or demonstrated 23 (on the detection sensor 1)  $\text{Fe}_3\text{O}_4$  nanoparticles have a total magnetic moment of  $\sim 11$  or 17 femu at the peaks of  $\Delta R$ , respectively, which is one order of magnitude lower than the prior reported detection limit of one 250-nm magnetic label or 200 femu [6]. Some clustering is noted in the deposited nanoparticles, as seen in Fig. 6, which might reduce the particle moments because of the inter-particle magnetostatic interaction [9]. In real biodetection applications, the nanoparticle labels would be more isolated due to the steric repulsion of attached biomolecules and surface surfactants. As a result of this separation, the detection sensitivity will be further enhanced. It is conceivable that an even lower number ( $< 10$ ) of nanoparticles will be detectable by using more sensitive sensors, such as magnetic tunnel junctions [28,29], and higher moment particles, such as Co and Fe, or by using lock-in detection to narrow the noise bandwidth.

In these experiments, more than one reference sensors were used to make certain that the resistance differences caused by the nanoparticles can be well distinguished. These reference sensors were randomly selected on the sensor chip, and were not necessarily the nearest neighbors of the detection sensors. Our experiments indicated that reference sensor signals were consistent among one another, and seemed uncorrelated to the sensor location on the chip. This implies that only a small portion of sensors may be needed as the reference for a large-scale integrated sensor array, leading to a high utilization ratio of the spin valve sensors for biodetection.

#### 4. Conclusions

Prototype GMR spin valve sensors have been designed and fabricated at a submicron scale for detection of magnetic nanoparticles intended as biomolecular labels in a mag-

netic biodetection technology. We demonstrate experimentally the detection of 16-nm superparamagnetic Fe<sub>3</sub>O<sub>4</sub> nanoparticles in various quantities from hundreds down to a few tens by spin valve sensors at room temperature. A linear relationship between sensor signal and nanoparticle quantity has been found. These experiments provide a direct proof of the feasibility of using submicron spin valve sensors as highly sensitive biosensors and monodisperse superparamagnetic nanoparticles as magnetic labels for emerging magnetic biodetection technology.

## Acknowledgements

The work was supported by the US Defense Advanced Research Projects Agency (DARPA) through US Navy grant no. N000140210807. The authors acknowledge fruitful discussions with Dr. D.B. Robinson, Dr. J.T. Kemp, Dr. H. Persson, Dr. C.D. Webb, and Prof. R.W. Davis at Stanford University, and support from other BioMagneticICs project members at Stanford and IBM. Assistance from Dr. Chang-Man Park is also gratefully acknowledged.

## References

- [1] D.R. Baselt, G.U. Lee, M. Natesan, S.W. Metzger, P.E. Sheehan, R.J. Colton, A biosensor based on magnetoresistance technology, *Biosens. Bioelectron.* 13 (1998) 731–739.
- [2] R.L. Edelstein, C.R. Tamanaha, P.E. Sheehan, M.M. Miller, D.R. Baselt, L.J. Whitman, R.J. Colton, The BARC biosensor applied to the detection of biological warfare agents, *Biosens. Bioelectron.* 14 (2000) 805–813.
- [3] M.M. Miller, P.E. Sheehan, R.L. Edelstein, C.R. Tamanaha, L. Zhong, S. Bounnak, L.J. Whitman, R.J. Colton, A DNA array sensor utilizing magnetic microbeads and magnetoelectronic detection, *J. Magn. Magn. Mater.* 225 (2001) 138–144.
- [4] D.L. Graham, H. Ferreira, J. Bernardo, P.P. Freitas, J.M.S. Cabral, Single magnetic microsphere placement and detection on-chip using current line designs with integrated spin valve sensors: biotechnological applications, *J. Appl. Phys.* 91 (2002) 7786–7788.
- [5] J. Schotter, P.B. Kamp, A. Becker, A. Puhler, D. Brinkmann, W. Schepfer, H. Bruckl, G. Reiss, A biochip based on magnetoresistive sensors, *IEEE Trans. Magn.* 38 (2002) 3365–3367.
- [6] H.A. Ferreira, D.L. Graham, P.P. Freitas, J.M.S. Cabral, Biodetection using magnetically labeled biomolecules and arrays of spin valve sensors (invited), *J. Appl. Phys.* 93 (2003) 7281–7286.
- [7] G. Li, V. Joshi, R.L. White, S.X. Wang, J.T. Kemp, C. Webb, R.W. Davis, S. Sun, Detection of single micron-sized magnetic bead and magnetic nanoparticles using spin valve sensors for biological applications, *J. Appl. Phys.* 93 (2003) 7557–7559.
- [8] D.L. Graham, H.A. Ferreira, P.P. Freitas, J.M.S. Cabral, High sensitivity detection of molecular recognition using magnetically labelled biomolecules and magnetoresistive sensors, *Biosens. Bioelectron.* 18 (2003) 483–488.
- [9] J.C. Rife, M.M. Miller, P.E. Sheehan, C.R. Tamanaha, M. Tondra, L.J. Whitman, Design and performance of GMR sensors for the detection of magnetic microbeads in biosensors, *Sens. Actuators A Phys.* 107 (2003) 209–218.
- [10] J. Schotter, P.B. Kamp, A. Becker, A. Puhler, G. Reiss, H. Bruckl, Comparison of a prototype magnetoresistive biosensor to standard fluorescent DNA detection, *Biosens. Bioelectron.* 19 (2004) 1149–1156.
- [11] G. Li, S.X. Wang, Analytical and micromagnetic modeling for detection of a single magnetic microbead or nanobead by spin valve sensors, *IEEE Trans. Magn.* 39 (2003) 3313–3315.
- [12] G. Li, S.X. Wang, S. Sun, Model and experiment of detecting multiple magnetic nanoparticles as biomolecular labels by spin valve sensors, *IEEE Trans. Magn.* 40 (2004) 3000–3002.
- [13] S.X. Wang, S.-Y. Bae, G. Li, S. Sun, R.L. White, J.T. Kemp, C.D. Webb, Towards a magnetic microarray for sensitive diagnostics, *J. Magn. Magn. Mater.* 293 (2005) 731–736.
- [14] D.B. Robinson, H.H.J. Persson, H. Zeng, G. Li, N. Pourmand, S. Sun, S.X. Wang, DNA-functionalized MFe<sub>2</sub>O<sub>4</sub> (M=Fe, Co, or Mn) nanoparticles and their hybridization to DNA-functionalized surfaces, *Langmuir* 21 (2005) 3096–3103.
- [15] K. Enpuku, T. Minotani, T. Gima, Y. Kuroki, Y. Itoh, M. Yamashita, Y. Katakura, S. Kuhara, Detection of magnetic nanoparticles with superconducting quantum interference device (SQUID) magnetometer and application to immunoassays, *J. Appl. Phys. Part 2 (Lett.)* 38 (1999) L1102–L1105.
- [16] Y.R. Chemla, H.L. Crossman, Y. Poon, R. McDermott, R. Stevens, M.D. Alper, J. Clarke, Ultrasensitive magnetic biosensor for homogeneous immunoassay, *Proc. Natl. Acad. Sci. U.S.A.* 97 (2000) 14268–14272.
- [17] Q.A. Pankhurst, J. Connolly, S.K. Jones, J. Dobson, Applications of magnetic nanoparticles in biomedicine, *J. Phys. D. Appl. Phys.* 36 (2003) R167–R181.
- [18] S. Sun, C.B. Murray, D. Weller, L. Folks, A. Moser, Monodisperse FePt nanoparticles and ferromagnetic FePt nanocrystal superlattices, *Science* 287 (2000) 1989–1991.
- [19] S. Sun, H. Zeng, D.B. Robinson, S. Raoux, P.M. Rice, S.X. Wang, G. Li, Monodisperse MFe<sub>2</sub>O<sub>4</sub> (M=Fe, Co, Mn) nanoparticles, *J. Am. Chem. Soc.* 126 (2004) 273–279.
- [20] B. Dieny, V.S. Speriosu, S. Metin, S.S.P. Parkin, B.A. Gurney, P. Baumgart, D.R. Wilhoit, Magnetotransport properties of magnetically soft spin-valve structures, *J. Appl. Phys.* 69 (1991) 4774–4779.
- [21] S.S.P. Parkin, D.E. Heim, Magnetoresistive spin valve sensor with improved pinned ferromagnetic layer and magnetic recording system using the sensor, US Patent 5,465,185 (1995).
- [22] R.R. Katti, Giant magnetoresistive random-access memories based on current-in-plane devices, *Proc. IEEE* 91 (2003) 687–702.
- [23] D.E. Heim, R.E. Fontana, C. Tsang, V.S. Speriosu, B.A. Gurney, M.L. Williams, Design and operation of spin valve sensors, *IEEE Trans. Magn.* 30 (1994) 316–321.
- [24] M.M. Miller, G.A. Prinz, S.F. Cheng, S. Bounnak, Detection of a micron-sized magnetic sphere using a ring-shaped anisotropic magnetoresistance-based sensor: a model for a magnetoresistance-based biosensor, *Appl. Phys. Lett.* 81 (2002) 2211–2213.
- [25] E.F. Ferrari, F.C.S. daSilva, M. Knobel, Influence of the distribution of magnetic moments on the magnetization and magnetoresistance in granular alloys, *Phys. Rev. B* 56 (1997) 6086–6093.
- [26] I. Hrianea, C. Caizer, Z. Schlett, Dynamic magnetic behavior of Fe<sub>3</sub>O<sub>4</sub> colloidal nanoparticles, *J. Appl. Phys.* 92 (2002) 2125–2132.
- [27] S. Sun, S. Anders, H.F. Hamann, J.U. Thiele, J.E.E. Baglin, T. Thomson, E.E. Fullerton, C.B. Murray, B.D. Terris, Polymer mediated self-assembly of magnetic nanoparticles, *J. Am. Chem. Soc.* 124 (2002) 2884–2885.
- [28] S.S.P. Parkin, C. Kaiser, A. Panchula, P.M. Rice, B. Hughes, M. Samant, S.H. Yang, Giant tunnelling magnetoresistance at room temperature with MgO(100) tunnel barriers, *Nat. Mater.* 3 (2004) 862–867.
- [29] S. Yuasa, T. Nagahama, A. Fukushima, Y. Suzuki, K. Ando, Giant room-temperature magnetoresistance in single-crystal Fe/MgO/Fe magnetic tunnel junctions, *Nat. Mater.* 3 (2004) 868–871.

## Biographies

**Guanxiong Li** was a PhD student from 1999 to 2004 at Stanford University while this work was conducted. He received his bachelor's degrees in materials science and engineering and in electronics and computer technology from Tsinghua University, Beijing, China, 1991, master's degree in microelectronics and solid-state electronics from Shanghai Institute of Metallurgy, Chinese Academy of Science, 1999, and PhD in materials science and engi-

neering from Stanford University, 2005. Currently, he works for Western Digital Corporation as a magnetic read head process engineer.

**Shouheng Sun** is an associate professor in the Department of Chemistry of Brown University. He received his BSc from Sichuan University in 1984, MSc from Nanjing University in 1987, and PhD from Brown University in 1996 all in chemistry. Before joining Brown, he was a postdoctoral fellow and a research staff at IBM T.J. Watson Research Center from 1996 to 2004. His research interest is in chemical synthesis, self-assembly of monodisperse nanoparticles and their potential applications in biomagnetics, nanocomposites, information storage, and catalysis.

**Robert J. Wilson** is a senior research engineer in the Department of Materials Science & Engineering at Stanford University. He received his AB and PhD degrees in physics from the University of California at Berkeley and an MS degree from the University of Chicago. Before joining Stanford, Wilson was with the IBM Almaden Research Center where he conducted research on surface and interface structure, nucleation and growth of thin films of atoms and molecules, and magnetic multilayer structures. His current research interests include nanomagnetics, nanofabrication techniques, and applications of nanotechnology in biology and medicine.

**Robert L. White** is a professor emeritus of electrical engineering and of materials science and engineering at Stanford University. He received his BA, MA, and PhD degrees in physics from Columbia University. He was on the scientific staff of Hughes Research Laboratories and of the General Telephone and Electronics Laboratory before joining the faculty at Stanford. He was chairman of the Department of Electrical Engineering from 1981 to 1987, and held the William E. Ayer Endowed Chair in Electrical Engineering. From 1987 to 1990 he was director of the Exploratorium Science Museum in San Francisco. His research interests are in magnetic materials and the physics of magnetism, neuroelectronic prostheses, particularly the cochlear prosthesis for the profoundly deaf, and in the application of magnetic nanoparticles to genetic analysis. He has 160 refereed publications, has written one book, and edited two others. He was founder and director of the Institute for Electronics in Medicine at Stanford and of the Stanford Center for Research on Information Storage Materials. He is a fellow of the American Institute of Physics and of the Institute of Electrical and Electronic Engineers. He has held fellowships or visiting professorships at the University of Tokyo, Oxford University, the Swiss Federal Institute of Technology (ETH), the Toyota Technological Institute, and the National University of

Singapore. He has been active in venture capital, and participated in seven start-up companies. He has been a consultant to the US Navy and to a number of companies, and is on a number of advisory and evaluation boards.

**Nader Pourmand** currently serves as senior research scientist in the Department of Biochemistry, Stanford Genome Technology Center, at Stanford University and leads the Bio-electrical and Pathogen detection laboratory. His main interest is to discover and develop novel methods for genetic analysis. In 1999, he obtained his PhD in experimental medicine and rheumatology from the Karolinska Institute in Sweden; and then joined the Stanford Genome Technology Center and developed pyrosequencing as a method for viral typing and for multiplex analysis of DNA samples. He has also been involved in Genotyping by a Co-Spotted Single-Base Extension Assay. In 2001, he invented a new chip-based DNA sequencing technology, Charge-Perturbation Signature (CPS): a new technique for DNA sequencing by utilizing charge-detection of extension. In addition to CPS he developed Bioluminescence Regenerative Cycle (BRC) system for nucleic acid quantification. He also refined and applied Molecular Inversion Probe for pathogen genotyping. He recently invented a Branch-Migration assay for short tandem repeats detection in forensic DNA fingerprinting.

**Shan X. Wang** currently serves as the director of the Center for Research on Information Storage Materials (CRISM), and is an associate professor in the Department of Materials Science & Engineering and jointly in the Department of Electrical Engineering at Stanford University. He is also with the Geballe Laboratory for Advanced Materials, and is affiliated with Stanford Bio-X Program. He received the BS degree in physics from the University of Science and Technology of China in 1986, the MS in physics from Iowa State University in 1988, and the PhD in electrical and computer engineering from the Carnegie Mellon University (CMU) at Pittsburgh in 1993. His current research interests lie in magnetic nanotechnologies in general and include bio-magnetic sensing, magnetic microarrays, novel magnetic nanoparticles, magnetoresistive materials and spin electronics, magnetic inductive heads and soft magnetic materials, as well as magnetic integrated inductors. He has published over 100 papers and holds 8 patents (issued and pending) on these subjects. He and Alex Taratorin also published a book titled "Magnetic Information Storage Technology" through Academic Press. Wang was among the inaugural group of Frederick Terman Faculty Fellows at Stanford University (1994–1997), and was an IEEE Magnetics Society Distinguished Lecturer (2001–2002).